

The First Photometric and Orbital Period Investigation of an Extremely Low Mass Ratio Contact Binary with a Sudden Period Change, TYC 4002-2628-1

Di-Fu. Guo,^{1*} Kai Li,^{1†} Fen Liu,¹ Huai-Zhen Li² Qi-Qi Xia,¹ Xing Gao,³ Xiang Gao,¹ Xu Chen,¹ Dong-Yang Gao,¹ and Guo-You Sun⁴

¹Shandong Provincial Key Laboratory of Optical Astronomy and Solar-Terrestrial Environment, Institute of Space Sciences, Shandong University, Weihai 264209, China

²Department of Physics, Yuxi Normal University, Yuxi, Yunnan, 653100, China

³Xinjiang Astronomical Observatory, 150 Science 1-Street, Urumqi 830011, China

⁴Wenzhou Astronomical Association

Accepted XXX. Received YYY; in original form ZZZ

ABSTRACT

Photometric observations for the totally eclipsing binary system TYC 4002-2628-1, were obtained between November 2020 and November 2021. To determine the stellar atmospheric parameters, a spectral image was taken with the 2.16 m telescope at National Astronomical Observatory of China (NAOC). TYC 4002-2628-1 is a low-amplitude (about 0.15 mag for V band), short-period (0.3670495 d), contact eclipsing binary with a total secondary eclipse. Intrinsic light curve variations and the reversal of the O’Connell effect are detected in the light curves, which may be due to spot activity. Based on the photometric solutions derived from the multi-band time series light curves, TYC 4002-2628-1 is an extremely low mass ratio contact binary with a mass ratio of $q \sim 0.0482$ and a fill-out factor of $f \sim 5\%$. By analyzing the $O - C$ variations, we find that its orbital period remains unchanged when $\text{BJD} < 2458321$. Then the orbital period changed suddenly around $\text{BJD} 2458743$ and has an increasing rate of $dP/dt = 1.62 \times 10^{-5} \text{ day} \cdot \text{yr}^{-1} = 140 \text{ second} \cdot \text{century}^{-1}$. If confirmed, TYC 4002-2628-1 would be the contact binary with the highest orbital period increasing rate so far. By investigating the ratio of orbital angular momentum to the spin angular momentum ($J_{orb}/J_{spin} < 3$), the instability mass ratio ($q_{inst}/q = 1.84$) and the instability separation ($A_{inst}/A = 1.35$), TYC 4002-2628-1 can be regarded as a merger candidate.

Key words: stars: binaries : close – stars: binaries : eclipsing – stars: evolution – stars: individual : TYC 4002-2628-1

CONTENTS

- 1 Introduction
- 2 Observations and data reduction
 - 2.1 Photometric observations
 - 2.2 Spectral observation
- 3 Orbital Period Investigation
- 4 Photometric Solutions
- 5 Discussions and Conclusions
 - 5.1 The period changes
 - 5.2 Potential of merger
- Acknowledgements

1 INTRODUCTION

W UMa binaries are short-period and low-temperature binary systems, with the two components over-filling their respective critical Roche lobe and sharing a common envelope. At the same time, the light curves are generally asymmetric and the maxima are usually unequal. The difference of the maximum values of the light curve, often caused by the strong magnetic activity (star spot) due to the deep convective envelopes, is usually referred to O’Connell effect (O’Connell 1951). Among W UMa binaries, deep (degree of overcontact $f > 50.0\%$), low mass ratio (mass ratio $q < 0.25$) overcontact binary systems play quite a critical role for studying and understanding the dynamical evolution of binaries since they are at late evolutionary stage, and may merge into rapidly rotating stars (Qian et al. 2005). Such stellar mergers are very rare, occurring about once every decade in our galaxy (Kochanek et al. 2014). So far, only one binary merging event, V1309 Sco (Tylenda et al. 2011; Zhu et al. 2016), has been found. Searching for such merger candidates of contact binary is quite important for studying stellar astrophysics.

Theoretical study indicates that a tidal instability would happen (Darwin’s instability) in a contact binary system when the mass ratio is less than the theoretical limit, which ultimately drives the system to

* E-mail: difu@sdu.edu.cn

† E-mail: kaili@sdu.edu.cn

evolve into a single, rapidly rotating object (Hut 1980). If this is the case, it may imply that such systems would not be observed. Based on different theoretical assumptions, the minimum mass ratio of contact binaries have been investigated by several authors. Rasio (1995) suggested that the lowest mass ratio for contact binaries possessing two unevolved main sequence stars is $q_{min} \simeq 0.09$. Li & Zhang (2006) derived a smaller value of $q_{min} \simeq 0.076$ by supposing W UMa systems rigorously comply with the Roche geometry. Arbutina (2007) found that the theoretical minimum mass ratio is ranged from 0.094 to 0.109. Later, Arbutina (2009) reanalyzed the minimum mass ratio by considering rotating polytropes and concluded q_{min} can achieve 0.070-0.074. On the basis of the primary structure and mass, Jiang et al. (2010) argued that the q_{min} can be as lower as 0.05. Up to now, only a few binaries have been found that the mass ratio is below 0.090, e.g., V1187 Herculis ($q \sim 0.044$, Caton et al. 2019), VSX J082700.8+462850 ($q \sim 0.055$, Li et al. 2021a), V857 Her ($q \sim 0.065$, Qian & Yang 2005), SX Crv ($q \sim 0.072$, Zola et al. 2004), ASAS J083241+2332.4 ($q \sim 0.068$, Sriram 2016), ZZ PsA ($q \sim 0.078$, Wadhwa et al. 2021), M4 V53 ($q \sim 0.078$, Li et al. 2017), NSV 13890 ($q \sim 0.080$, Wadhwa 2006), V870 Ara ($q \sim 0.082$, Szalai et al. 2007). Owing to their extremely low mass ratios around the theoretical limit, the discovery of such systems plays an important role in testing and constraining the theoretical evolutionary mode concerning binary mergers. However, due to the faintness of the less massive star, radial velocity (RV) determination for the extremely low mass ratio binaries is quite difficult. Total eclipsing binaries provide another channel to obtain reliable photometric solutions for the extremely low mass ratio systems without the need of the RV observations (Terrell & Wilson 2005; Li et al. 2021b).

W UMa stars are customarily classified into two subclasses: A-type and W-type (Binnendijk 1970), according to the shape of the light curve. For A-type binaries, the primary minimum is caused by the transit of the less massive component. On the contrary, the primary minimum of W-type binaries results from the occultation of the more massive component. However, some binaries, e.g., V857 Her (Qian et al. 2005), V802 Aql (Samec 2004), and RT LMi (Qian et al. 2008) reveal A-type light curves, but the photometric solutions show that the less massive components are hotter than the more massive ones, which imply W-type systems. In addition, a few contact binaries have changed their types among A and W at an interval of several years, like AM Leo (Binnendijk 1969; Hoffmann & Hopp 1982; Derman et al. 1991), AH Cnc (Maceroni et al. 1984; Zhang et al. 2005; Qian et al. 2006), SS Ari (Kim et al. 2003; Kurochkin 1960) and FG Hya (Qian & Yang 2005). These indicate that the type of a binary cannot be distinguished based on the shape of the light curve alone.

According to the International Variable Star Index ¹ (VSX) and the SIMBAD website ², the object TYC 4002-2628-1 (other names: CzeV710, UCAC4 725-101725, WISE J230927.8+545123) was first discovered as a binary by Heinze et al. (2018) with an extremely small amplitude of 0.138 mag (Chen et al. 2020). The orbital period of the target is 0.3670495 days. In this paper, the first complete BVR_cI_c band observations of TYC 4002-2628-1, exhibiting a total eclipse, are presented in Section 2. In Section 3, the orbital period variations were investigated based on the light minimum times. In Section 4, the photometric solutions were provided. Conclusion and discussion are summarized in Section 5.

2 OBSERVATIONS AND DATA REDUCTION

2.1 Photometric observations

Photometric observations of the total eclipse binary system TYC 4002-2628-1 were carried out from November 2020 to November 2021 with the 0.6m Ningbo Bureau of Education and Xinjiang Observatory Telescope (NEXT) and the 0.6m reflecting telescope at Weihai Observatory (WH60). A back illuminated FLI 230-42 CCD camera was mounted to the NEXT telescope. The camera has 2048×2048 square pixels with a field of view of $22' \times 22'$. As for WH60, SBIG STX-16803 was used to obtain the CCD images. The CCD possesses 4096×4096 square pixels with a field of view of $30' \times 30'$. The standard Johnson-Cousins filters (B , V , R_c , and I_c) were used during the observations. During each observing night, bias frames, dark frames and twilight sky flats were observed at the beginning or at the end of the observation. Otherwise, adjacent flat frames were used in the subsequent correction. Based on the IRAF software, the differential light curves were derived from aperture photometry. The finding chart and the basic information about the comparison star and the check star employed by us are exhibited in Figure 1 and Table 1, respectively. The exposure time for the observation obtained by NEXT is 30 s for V , 8 s for R_c and 12 s for I_c , respectively. While the typical exposure time for WH60 is 80 s for B , 25 s for R_c and 20 s for I_c , respectively.

To phase the light curves, the following ephemeris equation was used:

$$Min.I = HJD2459157.16588 + 0.3670495E. \quad (1)$$

According to the observation time and the shape of the light curves, three completed light curves (e.g., light curve one (LC_1) in 2020 November, light curve two (LC_2) in 2021 September and October, light curve three (LC_3) in 2021 November) were obtained, which are shown in Figure 2. From Figure 2, we can see that the light curves are varying with time, more or less, which may be caused by spot activities. To better compare the difference of light curve variations, the three I -band Light curves of TYC 4002-2628-1 are shown in the left panel of Figure 3 as an illustration. Based on Figure 3, the variations of the three sets of light curves are obvious, especially at primary maximum and secondary minimum. A positive O'Connell effect can be found in LC_1 , while LC_3 shows an obvious negative O'Connell effect. These indicate that the magnetic activity of TYC 4002-2628-1 is relatively active.

We searched for the Transiting Exoplanet Survey Satellite (TESS; Ricker et al. 2015) observation data of the target, and found it was observed during Sectors 16, 17, and 24 at 30-minute cadence. The Pre-search Data Conditioning Simple Aperture Photometry (PDC-SAP) flux values (F_i) of the target can be derived from the Mikulski Archive for Space Telescopes (MAST)³. Then we converted the flux to magnitudes (m_i), using the following equation: $m_i = -2.5 \log(F_i)$. The TESS magnitude of 10.78 derived from the fits head was used during the derivation of the magnitudes. Local eclipsing minima were used to fold the light curves, which are exhibited in the right panel of Figure 3. The intrinsic variations of the of light curves among different sectors are obvious, especially at the maxima and secondary minimum. A negative O'Connell effect can be found during Sectors 16 and then changes to positive in Sector 17. While a reversal of the O'Connell effect was found in Sector 24.

¹ <https://www.aavso.org/vsx/index.php>

² <http://simbad.cds.unistra.fr/simbad/>

³ <https://archive.stsci.edu/>

Table 1. Main parameters of TYC 4002-2628-1 and the reference stars.

Targets	name	α_{2000}	δ_{2000}	V_{mag}^*	$B - V$
Variable(V)	TYC 4002-2628-1	$23^h 09^m 27^s .87$	$+54^\circ 51' 23'' .5$	11.52	0.72
The comparison (C)	GSC 0400202568	$23^h 09^m 07^s .66$	$+54^\circ 52' 08'' .0$	11.70	0.76
The check (Ch)	GSC 0400202542	$23^h 09^m 05^s .87$	$+54^\circ 50' 33'' .0$	12.37	0.56

Note * Magnitudes were taken from the catalog of APASS DR9 (Henden et al. 2016).

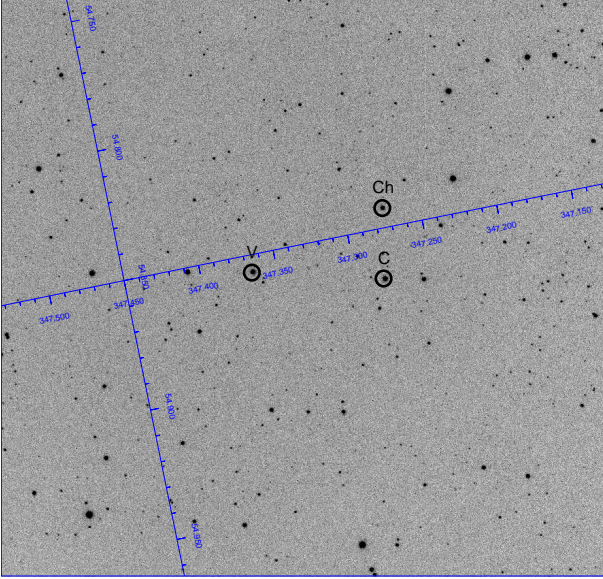


Figure 1. The middle area of the CCD image obtained by the Weihai 60cm telescope is used as the finding chart, TYC 4002-2628-1 (V), comparison (C) and check (Ch). The field of view is about $12' \times 12'$

2.2 Spectral observation

To estimate the temperature of the primary star, on January 5, 2022, a spectral image of the target at phase 0.55 was taken by the Beijing Faint Object Spectrograph and Camera (BFOSC) mounted on the 2.16-m telescope at NAOC. During the observation, low-dispersion spectrometer BFOSC and grism G4 were used, and the spectral resolution of a single pixel was 4.45 \AA (Fan et al. 2016). The IRAF software was applied to process the spectral data and extract the spectrum. After that the University of Lyon Spectroscopic analysis Software (ULySS) (Koleva et al. 2009) was applied to derive the atmospheric parameters of the system. The template spectra used for fitting are derived from an interpolator with the ELODIE library (Prugniel & Soubiran 2001). The normalized spectrum and the fitting spectrum are illustrated in Figure 4. The determined atmospheric parameters are as follows: $T_{eff} = 6032 \pm 26 \text{ K}$, $\log g = 4.3 \pm 0.06 \text{ cm s}^{-2}$, $[\text{Fe}/\text{H}] = 0.019 \pm 0.04 \text{ dex}$.

3 ORBITAL PERIOD INVESTIGATION

In order to study the orbital period variation of TYC 4002-2628-1, we use the optical sky survey data, i.e., Wide Angle Search for Planets (SuperWASP; Butters et al. 2010), All-Sky Automated Survey for SuperNovae (ASAS-SN; Shappee 2014; Jayasinghe et al. 2018), Wide-field Infrared Survey Explorer (WISE, Chen et al. 2018) and

the Transiting Exoplanet Survey Satellite (Ricker et al. 2015), to calculate its minimum times with the K-W method (Kwee & Woerden 1956). Due to the low time resolution of WISE, ASAS-SN and TESS (30 min for TYC 4002-2628-1), we have used the method of Li et al. (2020, 2021a) to compute the eclipsing minima. 46 new eclipsing minima were determined, which are illustrated in Table 2. In order to coincide with TESS time, HJD were transformed to BJD by using online tables⁴ (Eastman et al. 2010). Then the following equation:

$$\text{Min.I}(\text{BJD}) = 2459157.166669 + 0.3670495E \quad (2)$$

was applied to calculate the $O - C$ values. Based on Equation 2, the $O - C$ values are derived and illustrated in the left panel of Figure 5. As shown from the left panel of Figure 5, the $O - C$ values can be split into two parts. The first part of $O - C$ values (ranging from BJD 2454318 to 2458321) show an obvious linear variation, which may indicate the inaccuracy of the period. In order to correct this inaccuracy, the equation after the linear correction is as follows:

$$\text{Min.I}(\text{BJD}) = 2459157.158969(\pm 0.002398) + 0.3670474(\pm 0.000001)E \quad (3)$$

The recalculated values of $O - C$ derived from Equation 3 are shown in the right panel of Figure 5. From the right panel of Figure 5, the second part of $O - C$ values (ranging from BJD 2458743 to 2459525) show a parabolic variation, and the following equation was obtained:

$$\text{Min.I}(\text{BJD}) = 2459157.167537(\pm 0.001038) + 0.3670518(\pm 0.0000001)E + 8.124(\pm 1.137) \times 10^{-9} \times E^2. \quad (4)$$

The residuals are illustrated in the bottom of the right panel of Figure 5, where no obvious variations were found. The ephemeris shows a secular period increase which is determined to be $dP/dt = 1.62 \times 10^{-5} \text{ day} \cdot \text{yr}^{-1}$. The black line in Figure 5 refers to the fitting curve derived from the quadratic fit.

4 PHOTOMETRIC SOLUTIONS

The photometric solutions of TYC 4002-2628-1 were derived from the Wilson-Devinney (W-D) program of 2013 version (Wilson & Devinney 1971; Wilson 1990; Van Hamme & Wilson 2007; Wilson 2008; Wilson et al. 2010; Wilson 2012). The temperature T_{eff} obtained by the spectral fitting is close to the temperature ($T_{B-V} = 5942 \text{ K}$) derived from the $B - V$ color index after the correction of interstellar extinctions (Green et al. 2018). TYC 4002-2628-1 is an extremely low mass ratio contact binary, the more massive star provides most of the luminosity to the whole system. Meanwhile, the target is a total eclipse at the secondary minimum, and the spectrum was observed at 0.55 phase. Therefore the temperature (6032 K) derived from spectral fitting was used as the temperature of the more

⁴ <https://astroutils.astronomy.osu.edu/time/hjd2bjd.html>

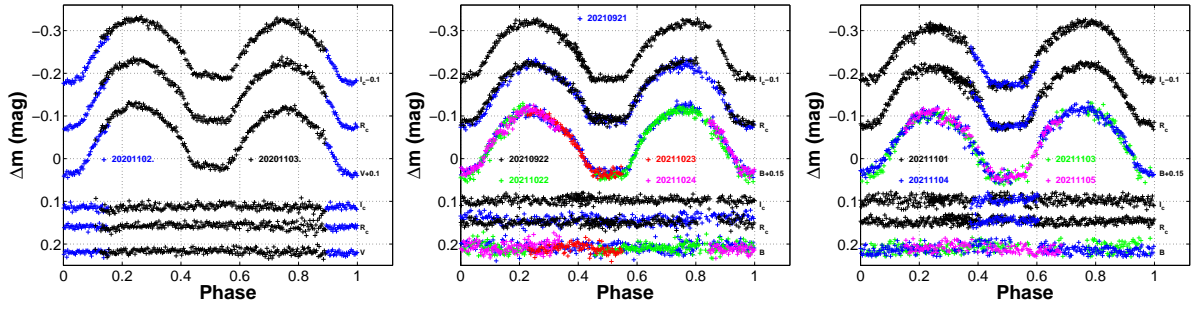


Figure 2. Multi-band light curves of TYC 4002-2628-1. The left panel is LC_1 observed in 2020 November, the middle panel is LC_2 observed in 2020 September and October, while the right panel is LC_3 obtained in 2021 November. The difference magnitudes of the comparison star and the check star are displayed at the bottom of the corresponding panel (constants added).

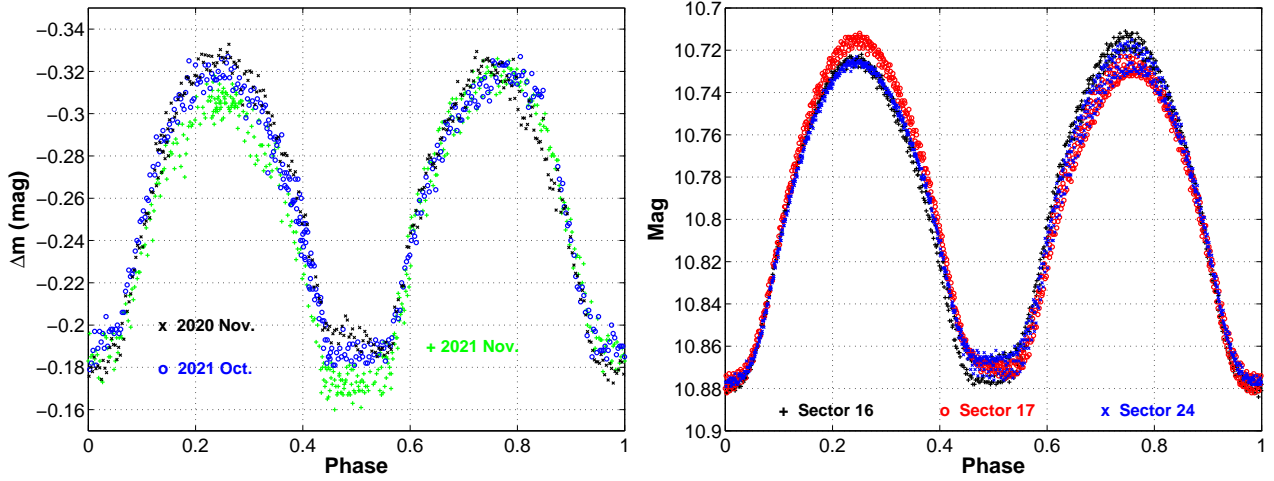


Figure 3. Comparison of the light curves observed at different times. The left panel shows the light curves of I_c band, while the right panel shows the light curves of TESS.

Table 2. CCD times of light minimum for TYC 4002-2628-1.

HJD +2450000	BJD +2450000	Error (days)	Min.	E	O-C(day)	HJD+2450000	BJD +2450000	Error (days)	Min.	E	O-C(day)
4318.55593 ^a	4318.556693	±0.00197	II	-13182.5	0.00059	8320.84124 ^d	8320.842050	±0.00263	II	-2278.5	0.00068
4344.61455 ^a	4344.615313	±0.00126	II	-13111.5	-0.00116		8743.87776 ^e	±0.00015	I	-1126	0.01421
4347.55056 ^a	4347.551323	±0.00100	II	-13103.5	-0.00153		8744.05989 ^e	±0.00022	II	-1125.5	0.01282
4351.58647 ^a	4351.587233	±0.00113	II	-13092.5	-0.00314		8757.45752 ^e	±0.00015	I	-1089	0.01322
4360.58289 ^a	4360.583653	±0.00067	I	-13068	0.00062		8757.64069 ^e	±0.00023	II	-1088.5	0.01286
4361.49939 ^a	4361.500153	±0.00081	II	-13065.5	-0.00050		8769.93655 ^e	±0.00017	I	-1055	0.01263
4363.51941 ^a	4363.520172	±0.00091	I	-13060	0.00076		8770.12300 ^e	±0.00022	II	-1054.5	0.01556
4364.43785 ^a	4364.438612	±0.00109	II	-13057.5	0.00158		8783.51542 ^e	±0.00016	I	-1018	0.01075
4371.59384 ^a	4371.594602	±0.00151	I	-13038	0.00014		8783.70197 ^e	±0.00022	II	-1017.5	0.01378
4372.51309 ^a	4372.513852	±0.00092	II	-13035.5	0.00177		8961.16365 ^e	±0.00014	I	-534	0.00802
4374.52892 ^a	4374.529682	±0.00067	I	-13030	-0.00116		8961.34852 ^e	±0.00029	II	-533.5	0.00937
4381.50481 ^a	4381.505572	±0.00095	I	-13011	0.00083		8974.74480 ^e	±0.00015	I	-497	0.00842
4382.42001 ^a	4382.420772	±0.00083	II	-13008.5	-0.00159		8974.92769 ^e	±0.00020	II	-496.5	0.00778
4393.43500 ^a	4393.435762	±0.00109	II	-12978.5	0.00198	9156.24990 ^f	9156.250689	±0.00054	II	-2.5	0.00934
4397.47422 ^a	4397.474982	±0.00110	II	-12967.5	0.00368	9157.16588 ^f	9157.166669	±0.00033	I	0	0.00771
4405.36130 ^a	4405.362062	±0.00110	I	-12946	-0.00076	9479.07808 ^g	9479.078860	±0.00030	I	877	0.01807
5390.88365 ^b	5390.884412	±0.00219	I	-10261	-0.00078	9479.26216 ^g	9479.262940	±0.00043	II	877.5	0.01985
5391.06672 ^b	5391.067482	±0.00420	II	-10260.5	-0.00124	9479.99632 ^g	9479.997100	±0.00034	II	879.5	0.01991
6857.60585 ^b	6857.606632	±0.00197	I	-6265	-0.00013	9480.17764 ^g	9480.178420	±0.00029	I	880	0.01771
6857.78939 ^b	6857.790172	±0.00136	II	-6264.5	-0.00011	9520.18901 ^g	9520.189789	±0.00037	I	989	0.02091
7240.43348 ^c	7240.434280	±0.00087	I	-5222	-0.00296	9522.94074 ^g	9522.941519	±0.00046	II	996.5	0.01978
7532.97111 ^d	7532.971914	±0.00212	I	-4425	-0.00213	9523.12551 ^g	9523.126289	±0.00034	I	997	0.02103
7533.16062 ^d	7533.161424	±0.00126	II	-4424.5	0.00385	9524.04374 ^g	9524.044519	±0.00044	II	999.5	0.02164
8320.65776 ^d	8320.658570	±0.00080	I	-2279	0.00072						

Note (a) SuperWASP, (b) WISE, (c) CzeV, (d) ASAS-SN, (e) TESS, (f) NEXT, (g) WH60.

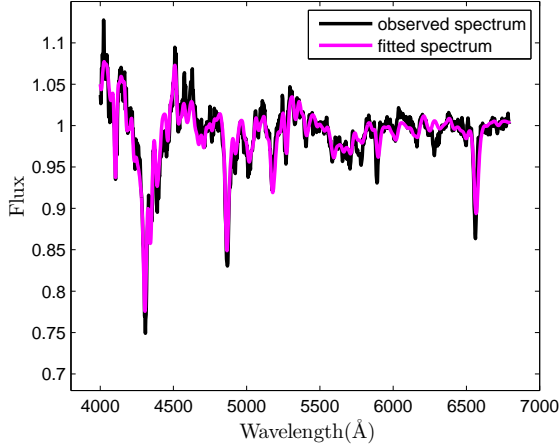


Figure 4. The observed and fitted spectrum of TYC 4002-2628-1.

Table 3. Photometric solutions of TYC 4002-2628-111

Parameters	Sol _{BVRI}	Sol _{TESS}
t_0	9479.077975 ^a	1743.877075 ^b
P_{ZERO}	0.3670584143	0.3670388842
T_1 (K)	6032	6032
T_2 (K)	6044(6)	6151(3)
$q(M_2/M_1)$	0.0482(1)	0.0482(fixed)
i (°)	69.9(1)	69.7(1)
Ω_{in}	1.782	1.782
Ω_{out}	1.750	1.750
$\Omega_1 = \Omega_2$	1.780(1)	1.771(1)
f	5(4)%	35(2)%
r_1	0.636(1)	0.641(1)
r_2	0.166(2)	0.173(1)
$\Sigma\omega(O - C)^2$	0.002015	0.0000032

Note (a) HJD-2450000, (b) BJD-2457000.

Table 4. Luminosity ratio and spot parameters derived from the *BVRI* light curves

Parameters	Sol.1 (LC_1)	Sol.2 (LC_2)	Sol.3 (LC_3)
$L_1/(L_1 + L_2)(B)$		0.9344(9)	0.9344(7)
$L_1/(L_1 + L_2)(V)$	0.9348(9)		
$L_1/(L_1 + L_2)(R)$	0.9349(6)	0.9349(8)	0.9349(1)
$L_1/(L_1 + L_2)(I)$	0.9350(5)	0.9350(9)	0.9350(10)
Colatitude(radian)	2.7449(401)	1.8300(27)	0.4735(121)
Longitude(radian)	0.4137(347)	4.77498(317)	4.2472(223)
Radius(radian)	0.7861(50)	0.3011(101)	0.24632(121)
T_s/T	0.9269(72)	0.9869(57)	0.92678(51)

massive star in the following analysis. The gravity darkening coefficients for the elements were fixed to be $g_1 = g_2 = 0.32$ (Lucy 1967) and the values of bolometric albedo coefficients $A_1 = A_2 = 0.5$ (Ruciński 1969). While the bandpass limb-darkening and the bolometric coefficients of the two stars were obtained from van Hamme's table (Van Hamme 1993).

Owing to lack of the radial velocity (RV) data, the q -search method was applied to get the initial mass ratio. The initial mass ratio can be

obtained as follows: firstly, consecutive photometric solutions were calculated for a series of mass ratios, then the relationship between the tested mass ratios and the mean residuals were derived. For comparison, the results of the q -search method derived from the three set multi-color light curves were illustrated in Figure 6. As can be seen from Figure 6, the minimum values for LC_1 , LC_2 and LC_3 are $q=0.048$, $q=0.043$ and $q=0.047$, respectively. If the light curves of the binary obtained at different times remain unchanged, the results of q -search should be identical. Nevertheless, the light curves always varies with time, more or less, due to various reasons. Among them, the spot activities on the star surface is the most common reason. So the results of the q -search method derived from the light curves are slightly different. At the same time, we also used the time series light curves to obtain the initial mass ratio. During the procession, the zero point of the orbital ephemeris (t_0), the orbital period (P_0), inclination (i), potential (Ω), temperature of the secondary (T_2) and luminosity of the primary (L_1) were the adjustable parameters. The results of the q -search method are displayed in Figure 7. From this figure, we can see that the minimum mass ratio is the same as the one derived from LC_1 , both of which are 0.048. Since LC_1 observed by NEXT is more homogeneous than the other two (LC_1 and LC_2), the minimum value $q=0.048$ was set as the initial mass ratio and set as an adjustable parameter in the following photometric solutions.

To generate a unique set of orbits and binary parameters consistent with each curve, we solved the multi-band time series light curves simultaneously using the 2013 version of the Wilson-Devinney program. As displayed in Figures 2 and 3, the light curves are asymmetric, which may be due to magnetic activities, so a star spot is added in each corresponding interval of time. The time spans corresponding to the three sets of light curves (LC_1 , LC_2 and LC_3) are used to define the active time of each spot in the subsequent photometric solution. Each spot is set to be active only for the corresponding time span, and spot parameters are adjusted to alternate between the three spots. After some interaction, the final solutions for the light curves were derived and listed in Table 3 as Sol_{BVRI}, and the spot parameters are shown in Table 4. The fitted light curves derived from the photometric solutions are displayed as solid lines in Figure 8, in which residuals (observed minus calculated light curves) from the solutions are shown in black dots. Since the third light will affect the mass ratio of photometric solution, We try to check the existence of the third body via adding a third light during the photometric analysis. However, the value of third light is always negative. We also checked the Gaia website and found that the closest star to the target is about 6 arcsecond away, which is larger than the photometric aperture. At the same time, the magnitude of nearest star is 20.6 magnitude, much dimmer than our target (11.3, g mag). Therefore, the contribution of the third light can be ignored.

Based on the shapes of the light curves, five sets of light curves were obtained from the TESS data (Sectors 16, 17, and 24), which are shown in Figure 9. The time spans corresponding to these five sets of light curves are used to define the active time of each spot in the subsequent photometric solution. Considering the TESS data for TYC 4002-2628-1 are in a 30-minute cadence and the short period of the target, the phase smearing effect inevitably affects the photometric solutions, such as the contact degree, orbital inclination and other parameters (Zola et al. 2017). In order to reduce the influence of the phase smear effect, the control parameter NGA=3 (Number of Gaussian quadrature abscissa in phase or time smearing simulation) was used (Zola et al. 2017). Using the same method as above, the final photometric solutions for the time series light curves were obtained and exhibited in Table 3 as Sol_{TESS} and Table 5.

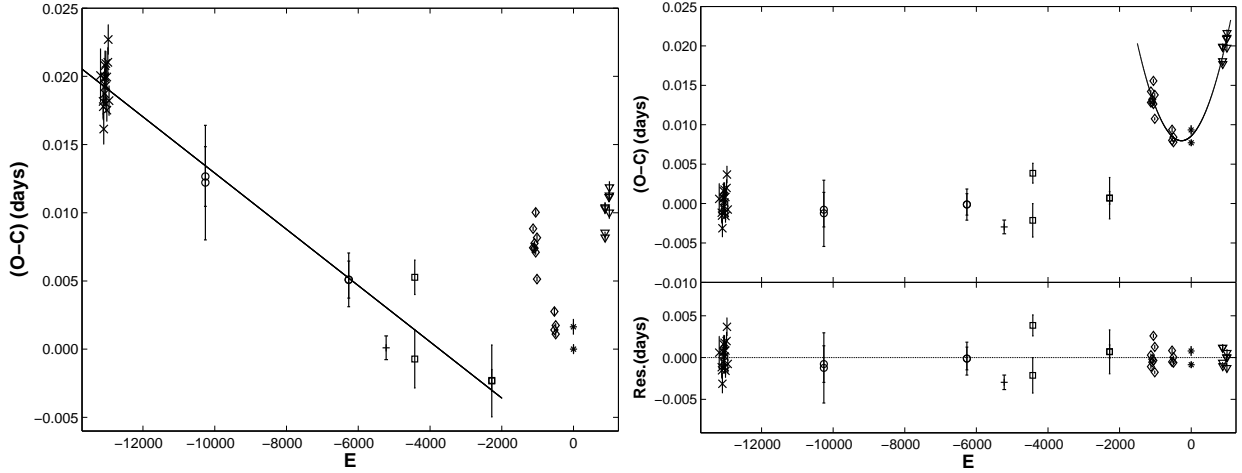


Figure 5. O-C diagram of TYC 4002-2628-1. x-mark, Superwasp; open circle, WISE; plus, CzeV; square, ASAS-SN; diamond, TESS; star, NEXT; triangle, WH60.

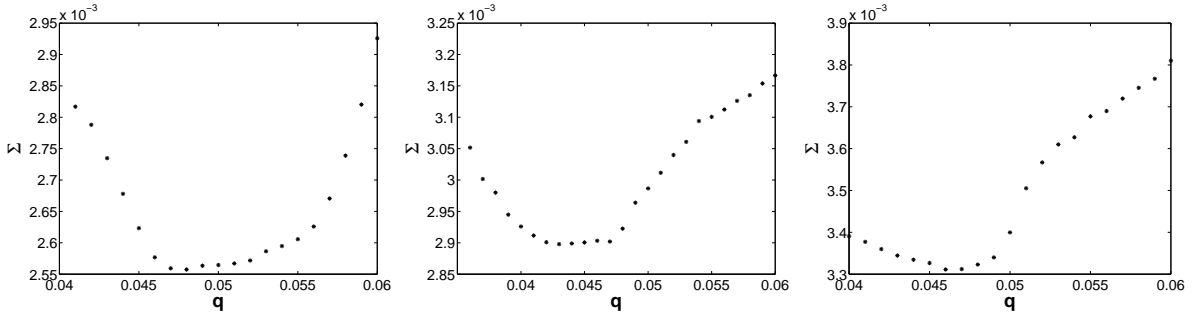


Figure 6. Mass ratio q vs mean residuals Σ for TYC 4002-2628-1 derived with the three light curves. The left panel, the middle panel and the right panel were derived from LC_1 , LC_2 and LC_3 , respectively.

Table 5. Luminosity ratio and spot parameters derived from the data of TESS

Parameters	Sector16-1	Sector16-2	Sector17	Sector24-1	Sector24-2
$L_1/(L_1 + L_2)$	0.9284(1)	0.9284(1)	0.9284(1)	0.9284(1)	0.9284(1)
Colatitude(radian)	0.0646(102)	0.0250(11)	0.0718(132)	0.1511(102)	0.1212(53)
Longitude(radian)	5.5173(133)	5.2820(452)	1.1281(136)	0.5388(136)	5.7113(195)
Radius(radian)	0.7266(19)	0.8122(fixed)	0.5038(33)	0.5725(9)	0.5315(6)
T_S/T	0.8806(8)	0.8773(fixed)	0.8114(7)	0.9691(9)	0.9150(6)

5 DISCUSSIONS AND CONCLUSIONS

Based on our observations and TESS data, eight complete light curves of TYC 4002-2628-1 were obtained. The light curves show day to day, month to month and year to year variations, indicating strong spot activities. As showed by the left panel of Figure 3, the secondary flat minimum (0.5 phase) is deeper than the primary minimum in LC_3 . This phenomenon implies that the binary system has changed its type (between W-type and A-type) in no more than one month. The light curves also show the reversal of O’Connell effect: Obvious positive O’Connell effects are found in LC_1 , LC_2 , Sector 17, and Sector 24-1, while other light curves show obvious negative O’Connell effect. Our photometric solutions indicate that the quick reversal of O’Connell effect can be explained by spot variation. All

these phenomena indicate the magnetic activity is very active, which may be due to the deep convective envelope along with rapid rotation.

The photometric solutions derived from the multi-band time series light curves indicate that TYC 4002-2628-1 is an extremely mass ratio contact binary, with a shallow contact degree of $f = (\Omega_{in} - \Omega)/(\Omega_{in} - \Omega_{out}) = 5\%$, where Ω_{in} is the potential when the Roche lobe arriving at Lagrange L_1 point of the system and Ω_{out} is the maximum potential of the Roche lobe (arriving at L_2) and Ω is the stars’ actual potential. The photometric solutions derived from different light curves are slightly different, which may be caused by the spot activity and the phase smearing effect. Supposing that the more massive component of the binary is a main-sequence star, we can estimate the mass of M_1 as $1.11 M_\odot$, according to the online

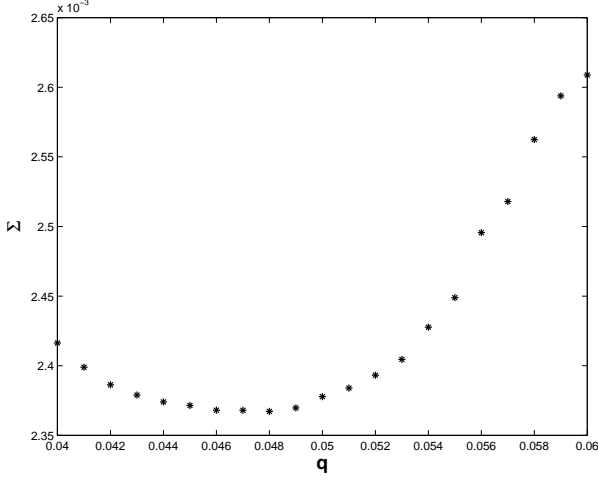


Figure 7. Mass ratio q vs mean residuals Σ for TYC 4002-2628-1 derived from the time series BVRI light curves.

table⁵ (Pecaut & Mamajek 2013). The less massive component of the target can be calculated as $M_2 = q \times M_1 = 0.0535 M_\odot$. According to Kepler's third law ($M = 0.0134a^3/P^2$), the distances between the two stars can be estimated as $a = 2.27R_\odot$. Based on the photometric solutions of LC_1 , the radii of the primary and secondary components can be calculated as $R_1 = r_1 \cdot a = 1.45R_\odot$, $R_2 = r_2 \cdot a = 0.39R_\odot$. The luminosity of $L_1 = 2.49L_\odot$ and $L_2 = 0.16L_\odot$ were derived from the Stefan-Boltzmann's law ($L = 4\pi\sigma T^4 R^2$).

5.1 The period changes

By analyzing all of the calculated eclipsing minima, the orbital period variation of TYC 4002-2628-1 can be divided into two parts (see Figure 5). The first part of the $O - C$ diagram reveals that the period remains unchanged, which indicate there was no mass exchange between the two components. The second part of the $O - C$ diagram shows a parabolic variation, which implies its period has changed suddenly. The discontinuity of the period may be caused by a sudden mass transfer between the two components. The quadratic term in Equation 4 implies that the period is long-term increasing at a rate of $dP/dt = 1.62 \times 10^{-5} \text{ day} \cdot \text{yr}^{-1}$ ($1.40 \text{ s} \cdot \text{yr}^{-1}$). If this is the case, TYC 4002-2628-1 would be the contact binary with the highest orbital period increasing rate so far. The long-term period increase can be explained by the mass transfer from less massive component to the more massive one. The rate of mass transfer can be derived from the formula,

$$\frac{\dot{P}}{P} = -3\dot{M}_1 \left(\frac{1}{M_1} - \frac{1}{M_2} \right), \quad (5)$$

by supposing the mass transfer is conservative. The decreasing rate for the less massive star is computed to be $dM_2/dt = 8.25 \times 10^{-7} M_\odot \text{ yr}^{-1}$. Considering the observation span for the parabolic variation of $O - C$ diagram is less than three years, the continuous period increase maybe just a part of the periodic variation. More eclipsing minima are required to test this possibility.

⁵ http://www.pas.rochester.edu/~emamajek/EEM_dwarf_UBVIJHK_colors_Teff.txt

5.2 Potential of merger

According to the theory of Darwins instability (Hut 1980), if $\frac{J_{spin}}{J_{orb}} > 1/3$, the contact binaries will move towards merger, where J_{spin} and J_{orb} represent the spin angular momentum and the orbital angular momentum, respectively. The value of $\frac{J_{spin}}{J_{orb}}$ can be derived from the following equation (Yang & Qian 2015):

$$\frac{J_{spin}}{J_{orb}} = \frac{1+q}{q} [(k_1 r_1)^2 + (k_2 r_2)^2 q], \quad (6)$$

where k_1 and k_2 are the dimensionless gyration radii of the corresponding components, r_1 and r_2 are the relative radii of the components. The value of k_1 was calculated using the equation: $k_1 = -0.250M + 0.539$ (Landin 2009; Christopoulou et al. 2022). Due to the very low mass of the less massive component, the value of k_2^2 was fixed as 0.205, which is consistent with a fully convective star (Arbutina 2007). By substituting the above values into Equation 6, we can get $\frac{J_{spin}}{J_{orb}} = 0.6210$, which is more than 1/3. For comparison, $k_1^2 = k_2^2 = 0.06$ (Rasio 1995; Li & Zhang 2006) was adopted to recalculate $\frac{J_{spin}}{J_{orb}}$. Then the value of $\frac{J_{spin}}{J_{orb}}$ can be determined to be 0.5380, which is still more than 1/3.

For further investigation of the stability of TYC 4002-2628-1, we have used the methods introduced by Wadhwa et al. (2021) to estimate the instability parameters. According to the mass of primary component (M_1) and the fill-out factor (f), the instability mass ratio q_{inst} was calculated as 0.086, which is larger than the mass ratio ($q \sim 0.0482$) derived from WD code. In order to estimate the instability separation (A_{inst}), k_1 was calculated using the equation: $k_1 = -0.250M + 0.539$ (Landin 2009; Christopoulou et al. 2022) and the value of k_2^2 was fixed to be 0.205 as mentioned above. Then $A_{inst} = 3.034R_\odot$ was determined. Both of the instability parameters (q_{inst} , A_{inst}) are larger than the actual parameters ($q = 0.0482$, $A = 2.27R_\odot$), indicating that the target is a potential merger candidate.

analyzing the light minimum times, a highest rate of orbital period increase ($dP/dt = 1.62 \times 10^{-5} \text{ day} \cdot \text{yr}^{-1} = 1.40 \text{ s} \cdot \text{yr}^{-1}$) was obtained. However, due to the short time span of observation, more eclipsing minima are needed to verify its authenticity. By studying the ratio of spin angular momentum to orbital angular momentum ($\frac{J_{spin}}{J_{orb}} > 1/3$), the instability mass ratio ($q_{inst} > q$)

In summary, the first multi-band photometric and spectral observations of the total eclipse binary TYC 4002-2628-1 were presented. The photometric solutions indicate the system is an extremely low mass ratio ($q \sim 0.0482$) with a shallow contact degree. So far, there is only one similar system with a mass ratio less than 0.05: V1187 Herculis. Searching for more such kind binaries will help us to test and constrain the merging theory. The $O - C$ diagram shows that the period of TYC 4002-2628-1 has changed suddenly $BJD2458743$. By and the instability separation ($A_{inst} > A$), we found that the system, like ZZ PsA, SX CrV, ASAS J165139+2255.7 and V1187 Her, is a candidate of merging binary.

ACKNOWLEDGEMENTS

This work is supported by the National Natural Science Foundation of China (NSFC) (No.12063005), and the Joint Research Fund in Astronomy (No. U1931103) under cooperative agreement between NSFC and Chinese Academy of Sciences (CAS), and by the Qilu Young Researcher Project of Shandong University, and by the Chinese Academy of Sciences Interdisciplinary Innovation Team, and

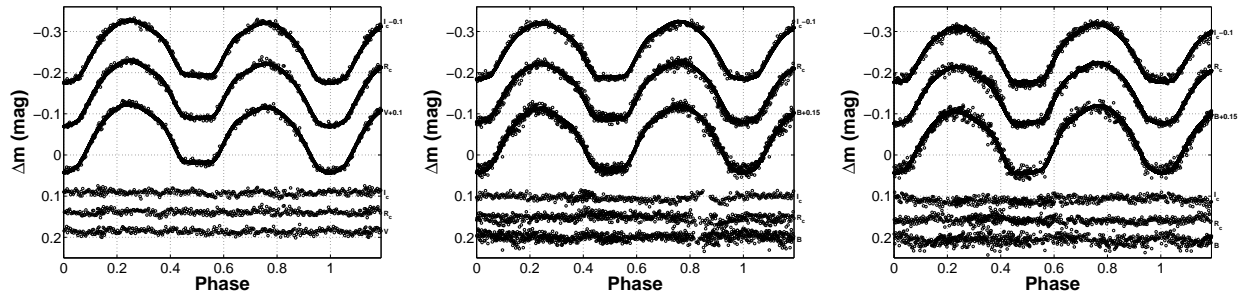


Figure 8. The theoretical light curves of TYC 4002-2628-1. The residuals are plotted at bottom of the corresponding panels. The left panel observed in 2020 November (LC_1), the middle panel observed in 2020 September and October (LC_2), while the right panel obtained in 2021 November (LC_3).

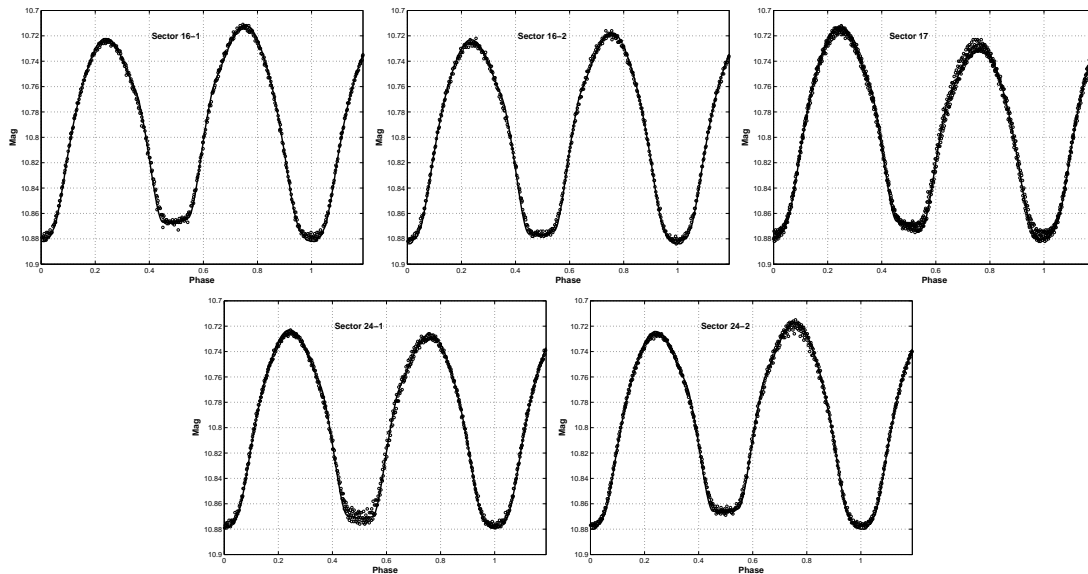


Figure 9. Light curves of TYC 4002-2628-1 obtained by TESS. The solid lines represent the theoretical light curves.

by the Cultivation Project for LAMOST Scientific Payoff and Research Achievement of CAMS-CAS, and the Program for Innovative Research Team (in Science and Technology) in the University of Yunnan Province (IRTSTYN), and Yunnan Local Colleges Applied Basic Research Projects (2019FH001-12). The calculations in this work were carried out at Supercomputing Center of Shandong University, Weihai. We acknowledge the support of the staff of the Xinglong 2.16m telescope. This work was partially supported by the Open Project Program of the CAS Key Laboratory of Optical Astronomy, National Astronomical Observatories, Chinese Academy of Sciences. Many thanks to anonymous reviewer for their very helpful comments and suggestions, which greatly improved our manuscript.

This work makes use of data collected by the TESS mission which are funded by NASA Science Mission directorate. We acknowledge the TESS team for its support of this work. This paper also used the data from ASAS-SN, which is funded in part by the Alfred P. Sloan Foundation under grant G202114192. This paper makes use of data from the DR1 of the WASP data (Butters et al. 2010) as provided by the WASP consortium, and the computing and storage facilities at the CERIT Scientific Cloud, reg. no. CZ.1.05/3.2.00/08.0144 which is operated by Masaryk University, Czech Republic.

DATA AVAILABILITY

The photometric data for the NEXT and WH60 used in this article are available in online supplementary material. The TESS data are publicly available at <http://archive.stsci.edu/te ss/bulk downloads.html>, SuperWASP data are publicly available at <https://wasp.cerit-sc.cz/search> and ASAS-SN data are publicly available at <https://asas-sn.osu.edu/variables/lookup>. The WISE data used in this paper are publicly available at <http://variables.cn:88/wise/>. The CzeV data used in this paper are derived from <http://var2.astro.cz/czev.php?id=710>.

REFERENCES

- Arbutina, B. 2007, MNRAS, 377, 1635
- Arbutina, B. 2009, MNRAS, 394, 501
- Binnendijk, L. 1969, AJ, 74, 1031
- Binnendijk, L. 1970, Vistas in Astronomy, 12, 217
- Butters, O. W., West, R. G., Anderson, D. R., et al. 2010, A&A, 520, L10
- Chen, X. D., Wang, S., Deng, L. C., et al., ApJS, 2020, 249:18
- Chen, X. D., Wang, S., Deng, L. C., et al., ApJS, 2018, 237:28
- Christopoulou, P. E., Lalounta, E., Papageorgiou, A., et al., MNRAS, 2022, 512,1244
- Caton, D., Gentry, D. R., Samec, R. G., et al., PASP, 2019, 131:054203
- Darwin, G. H. 1879, RSPS, 29, 168

- Derman, E., Demircan, O., & Dunder, H. 1991, *Information Bulletin on Variable Stars*, 3630, 1
- Eastman, J., Siverd, R., & Gaudi, B. S. 2010, *PASP*, 122, 935
- Fan, Z., Wang, H. J., Jiang, X. J., et al. 2016, *AJ*, 128, 115005
- Green, G. M., Schlafly, E. F., Finkbeiner, D., et al. 2018, *MNRAS*, 478, 651
- Henden, A. A., Templeton, M., Terrell, D., et al. 2016, *yCat*, 2336, 0
- Heinze, A. N., Tonry, J. L., Denneau, L., et al. 2018, *AJ*, 156, 241
- Hoffmann, M., & Hopp, U. 1982, *Ap&SS*, 83, 391
- Hut, P. 1980, *A&A*, 92, 167
- Jayasinghe, T., Kochanek, C. S., Stanek, K. Z., et al. 2018, *MNRAS*, 477, 3145
- Jiang, D., Han, Z., Wang, J., Jiang, T., & Li, L. 2010, *MNRAS*, 405, 2485
- Kim, C.-H., Lee, J. W., Kim, S.-L., Han, W., & Koch, R. H. 2003, *AJ*, 125, 322
- Kwee, K. K., & van Woerden, H. 1956, *BAN*, 12, 327
- Kochanek C. S., Adams S. M., Belczynski K., 2014, *MNRAS*, 443, 1319
- Koleva, M., Prugniel, P., Bouchard, A., & Wu, Y. 2009, *A&A*, 501, 1269
- Kurochkin, N. E. 1960, *Astronomicheskij Tsirkulyar*, 212, 9
- Landin, N. R., Mendes, L. T. S., & Vaz, L. P. R. 2009, *A&A*, 494, 209
- Li, K., Hu, S. M., Chen, X., & Guo, D. F. 2017, *PASJ*, 65, 79
- Li K. Kim C.-H., Xia Q.-Q., Michel R., Hu S.-M., Gao X., Guo D.-F., Chen X., 2020, *AJ*, 159, 189
- Li, K., Xia, Q. Q., Kim, C. H., et al. 2021, *ApJ*, 922, 122
- Li, K., Xia, Q. Q., Kim, C. H., et al. 2021, *AJ*, 162, 13
- Li, L., & Zhang, F. 2006, *MNRAS*, 369, 2001
- Lucy, L. B. 1967, *Z. Astrophys.*, 65, 89
- Maceroni, C., Milano, L., & Russo, G. 1984, *A&AS*, 58, 405
- O'Connell, D. J. K. 1951, *PRCO*, 2, 85
- Qian, S., & Yang, Y. 2005, *MNRAS*, 356, 765
- Qian, S.-B., Zhu, L.-Y., Soonthornthum, B., et al. 2005, *AJ*, 130, 1206
- Qian, S.-B., Liu, L., Soonthornthum, B., Zhu, L.-Y., & He, J.-J. 2006, *AJ*, 131, 3028
- Qian, S.-B., He, J.-J., & Xiang, F. Y. 2008, *PASJ*, 60, 77
- Rasio, F. A. 1995, *ApJ*, 444, L41
- Pecaut, M. J., & Mamajek, E. E. 2013, *ApJS*, 208, 9
- Ricker, G. R., et al. 2015, *J. Astron. Telescopes, Inst. Syst.*, 1, 014003
- Prugniel, P., & Soubiran, C. 2001, *A&A*, 369, 1048
- Ruciński, S. M. 1969, *Acta Astron.*, 19, 245
- Samec, R. G., Martin, M., & Faulkner, D. R. 2004, *IBVS*, 5527
- Shappee, B. J., Prieto, J. L., Grupe, D., et al. 2014, *ApJ*, 788, 48
- Sriram, K., Malu, S., Choi, C. S., & Vivekananda Rao, P. 2016, *AJ*, 151, 69
- Szalai, T., et al. 2007, *A&A*, 465, 943
- Terrell, D., Wilson, R. E. 2005, *Ap&SS*, 296, 221
- Van Hamme, W., & Wilson, R. E. 2007, *ApJ*, 661, 1129
- Van Hamme, W. 1993, *AJ*, 106, 2096
- Tylenda, R., Hajduk, M., Kamiński, T., et al. 2011, *A&A*, 528, 114
- Wadhwa, S. S. 2006, *Ap&SS*, 301, 195
- Wadhwa S. S., De Horta A. Y., Filipović M. D., et al. 2021, *MNRAS*, 501, 229
- Wilson, R. E. 1990, *ApJ*, 356, 613
- Wilson, R. E. 2008, *ApJ*, 672, 575
- Wilson, R. E. 2012, *AJ*, 144, 73
- Wilson, R. E., Devlinney E.J. 1971, *ApJ*, 166, 605
- Wilson, R. E., Van, Hamme. W., Terrell, D. 2010, *ApJ*, 723, 1469
- Yang, Y.-G., & Qian, S.-B. 2015, *AJ*, 150, 69
- Wozniak, P. R., Vestrand, W. T., Akerlof, C. W., et al. 2004, *AJ*, 127, 2436
- Zhang, X. B., Zhang, R. X., & Deng, L. 2005, *AJ*, 129, 979
- Zhu, L. Y., Zhao, E. G., Zhou, X. 2016, *RAA*, 16, 068
- Zola, S., Baran, A., Debski, B., & Jableka, D. 2017, *MNRAS*, 466, 2488
- Zola, S., et al. 2004, *Acta Astron.*, 54, 299

This paper has been typeset from a $\text{\TeX}/\text{\LaTeX}$ file prepared by the author.